Demonstration of Reduced False Alarm Rates using Simulated L-Band Polarimetric SAR Imagery of Concealed Targets

Mark L. Williams and Nicola Harris

Abstract—**Coherent scattering calculations have been performed to produce L-Band SAR images of targets below a forest canopy. The calculations, which are fully polarimetric, are described. High clutter levels permit detection of all concealed targets only at the cost of a very high false alarm rate. The simulated imagery is analysed using the entropy-alpha polarimetric decomposition technique. Using alpha and entropy in addition to a co-polar intensity channel, and combining the results of separate CFAR algorithms, the number of false alarms is reduced dramatically. The consequences for application of polarimetric SAR to concealed target detection and identification are considered.**

Index Terms—**Concealed target detection, polarimetric SAR, simulation.**

I. Introduction

The detection in SAR imagery of targets concealed by foliage requires substantial penetration of the forest canopy by microwave radiation. Vegetation generally contains a high water content, and is strongly absorbing at traditional SAR frequencies (e.g. X-band). Deep penetration into foliage can only be achieved at lower frequencies, for example at VHF or UHF [1-4]. The move to lower frequencies has a number of important consequences for SAR operation: lower frequency means that longer apertures are required to maintain resolution. Consequently observation times are extended, and SAR focus is made more difficult [2-4].

As the operational frequency decreases the fractional bandwidth must increase to maintain range resolution, and the effects of bandwidth are more noticeable in scattering responses. Radio bands at low frequencies, especially UHF and VHF, are cluttered with RFI from TV and communications sources, which can degrade or even prevent SAR image formation. However, progression to lower frequencies is marked by a desirable improvement in signal to clutter ratio, as dimensions of plant elements become progressively shorter than wavelengths.

Manuscript received January 1, 2003. This work has been funded by the UK MOD Corporate Research Programme under Technology Group 9 (RF Technology).

At the time of writing M L Williams was with DSTL, Malvern, UK, (phone: +44(0)1684-771398; fax: +44(0)1684-771434; e-mail: mlwilliams2@dstl.gov.uk) and is now with DSTO, Adelaide, SA.

Thus low frequencies provide good penetration, but provide challenges for SAR image formation, whilst high frequencies make SAR image formation easier, but yield poor penetration. Any technique that can help recover detection rates whilst permitting a high operational frequency is therefore desirable. One approach is to increase bandwidth at the high frequency end of the operational spectrum. Greater bandwidth yields lower clutter levels through improved resolution, and may thus permit attenuated target returns to be detected. Indeed anecdotal evidence suggests that simple calculations overestimate attenuation effects since they do not properly account for canopy inhomogeneity. Clear gaps and sparse canopy volumes work in favour of the detecting sensor.

An alternative approach, considered here, represents a compromise: lowering the operational frequency to L-band to increase foliage penetration, whilst increasing the amount of observed information by using a fully polarimetric SAR. It has been understood for some time that the polarimetric radar response of artificial targets differs in form from that of natural vegetation. Surrounding clutter will confuse the scattering matrix of a concealed target in a SAR image. However, polarimetric target decomposition theory [5] indicates that, even when the target signal is relatively weak, scattering behaviour associated with artificial targets may be identified using eigenvalue decomposition of the coherency matrix. At the same time, even though with good foliage penetration concealed targets may appear bright in co-polar SAR channels, co-polar clutter levels may frequently exceed target intensities. Taken independently co-polar intensity or polarimetric decomposition may only be used to detect concealed targets with high false alarm rates. However, by correlating detections in the co-polar channel with those in the polarimetric decomposition, one might achieve a reduction in false alarm rate.

In what follows we describe numerical calculations of SAR images of concealed targets *in-situ* beneath canopies of Scots Pine trees, and the analysis of simulated polarimetric SAR data. We correlate the CFAR detections on co-polar, alpha and entropy channels and show that by so doing four hidden targets can be detected without any false alarms. Finally we consider extension of this specific case to a more general methodology.

Report Documentation Page

Form Approved
OMB No. 0704-0188

1. REPORT DATE	2. REPORT TYPE	3. DATES COVERED
14 APR 2005	**N/A**	**-**

4. TITLE AND SUBTITLE	5a. CONTRACT NUMBER
Demonstration of Reduced False Alarm Rates using Simulated L-Band Polarimetric SAR Imagery of Concealed Targets	5b. GRANT NUMBER
	5c. PROGRAM ELEMENT NUMBER
6. AUTHOR(S)	5d. PROJECT NUMBER
	5e. TASK NUMBER
	5f. WORK UNIT NUMBER
7. PERFORMING ORGANIZATION NAME(S) AND ADDRESS(ES) **DSTL, Malvern, UK;**	8. PERFORMING ORGANIZATION REPORT NUMBER
9. SPONSORING/MONITORING AGENCY NAME(S) AND ADDRESS(ES)	10. SPONSOR/MONITOR'S ACRONYM(S)
	11. SPONSOR/MONITOR'S REPORT NUMBER(S)

12. DISTRIBUTION/AVAILABILITY STATEMENT
Approved for public release, distribution unlimited

13. SUPPLEMENTARY NOTES
See also ADM001798, Proceedings of the International Conference on Radar (RADAR 2003) Held in Adelaide, Australia on 3-5 September 2003., The original document contains color images.

14. ABSTRACT

15. SUBJECT TERMS

16. SECURITY CLASSIFICATION OF:			17. LIMITATION OF ABSTRACT	18. NUMBER OF PAGES	19a. NAME OF RESPONSIBLE PERSON
a. REPORT	b. ABSTRACT	c. THIS PAGE			
unclassified	**unclassified**	**unclassified**	**UU**	**6**	

II. CALCULATING SAR IMAGES OF CONCEALED TARGETS

A. General

The techniques employed for target calculations are similar to those used for SAR prediction in previous works at various frequencies [6,7]. The modelling of SAR imaging of the forest environment has been performed in the distorted-Born approximation and builds on previous work on RCS prediction for forests [8-14].

Proper numerical solution of Maxwell's equations for scattering calculations, using techniques such as the method of moments, may not be easily extended to the calculation of *in-situ* target signatures. The calculations performed here, although approximate in nature, represent a complement to more expensive yet limited techniques and extend the prediction capability to include high fidelity modelling of the target environment.

B. SAR Image Formation

Predicted SAR images are modelled as the coherent superposition of focused scattering events. These events may be considered to arise from elements of the scene, whether natural or artificial, with dimensions less than the scale of resolution. Thus a mathematical model for the coherent SAR image is

$$\underline{\underline{P}}(x_0, R_0) = \sum_j \underline{\underline{F}}_j \, \hat{Q}(x_0, R_0, \underline{s}_j), \qquad (1)$$

where in (1) $\underline{\underline{P}}(x_0, R_0)$ is the polarimetric pixel value at cross range x_0 and range R_0, $\underline{\underline{F}}_j$ is the polarimetric scattering amplitude associated with the scene element, and $\hat{Q}(x_0, R_0, \underline{s}_j)$ is the complex, phase containing, system point spread function depending upon the *effective* scattering centre $\underline{s}_j$.

Scattering amplitudes are calculated in various approximations depending upon their nature. These may be averaged both in along-track observation position and frequency over the respective SAR bandwidths in order to estimate better the observed return. Each scattering event may be shadowed by targets, and returns are attenuated by the forest canopy (if present), with variation in attenuation with along-track observation position (due to canopy inhomogeneity) and frequency (due to permittivity frequency dependence) taken into account when averaging. In addition the effects of antenna pattern may be incorporated in the calculations using a simple model for a dipole antenna, appropriate at very low frequencies (although not required at L-band). Scattering events fall into the following classes: direct-ground, direct-target, direct-forest, ground-target, ground-forest, ground-target-ground, and ground-forest-ground.

All target interactions contain up to third order multipath over the target, and ground-target-ground interactions can include up to four scattering surfaces (with the ground included twice). All volume terms originate from the forest canopy. This is modelled as tree structures described as collections of dielectric, absorbing cylinders and pine needles.

The (complex, phase containing) system point spread function is determined from SAR imaging geometry, bandwidth and processing options. The platform motion is ideal, and the platform is modelled as having a straight, uniform trajectory.

After first describing the scenario, the calculation proceeds by addressing each scattering element in turn. Each element has an associated "effective scattering centre". For first order returns this is simply the centre of the element. For higher order returns involving multiple reflections this effective scattering centre is determined rapidly at run-time using knowledge of the scattering path and the antenna motion [6].

The scattering amplitude associated with the element is then determined using an appropriate physical model. With the location and amplitude determined, and the form of the point-spread function (PSF) decided the contribution is summed coherently into all relevant pixel accumulators.

All calculations are performed using the Forward Scattering Alignment (FSA) [20] and simulated SAR images are output in ground range and azimuth.

C. Direct-Ground Scattering

A digital elevation map is interpolated and divided into triangular facets of sufficiently small size as to ensure fully developed speckle (typically an average of more than 10 per resolution cell). The small perturbation model (SPM) with Gaussian correlation [15] was adopted for the ground RCS. This model is coupled to ground permittivity, modelled as dependent upon soil moisture and frequency. The effective scattering centre is determined simply as the facet centre, and the centre of focus simply the projection of this point onto the SAR imaging plane. Local speckle statistics are assumed Gaussian. Polarimetric scattering amplitude values in the local frame are drawn from distributions using the mean RCS for the facet as determined from local incidence and speckle phase is added using an appropriate model. The scattering amplitude is scaled by attenuation tensors determined from line-of-sight visibility through the canopy, and averaged over frequency bandwidth and along-track observation position. The attenuation parameters depend upon the detail of canopy constitution and are calculated in the first order smoothing approximation based on knowledge of the scattering properties of the forest canopy. Shadowing of direct-ground returns by targets is accommodated in the calculation.

D. Target Scattering

The target is modelled as a collection of perfectly conducting, interacting surfaces with coded visibility [6,7]. Each of these surfaces is divided into triangular facets of dimension less than the system resolution. The scattering amplitude of a facet is modelled in the Geometrical Optics - Physical Optics (GO-PO) approximation.

Direct-target scattering can involve up to third order multipath over the target. The first and last surfaces in the scattering chain may be different, and so the incident and scattered attenuation dyadics may be different in direct-target terms.

We model multipath between ground and target when the ground is essentially locally flat (over the region traversed by the specular point) and only slightly rough. The ground is modelled as a rough dielectric surface, with Fresnel reflection coefficients scaled according to the surface roughness. The attenuation dyadic for the incident path is now calculated for transmission between the platform and the specular point on the ground surface.

If the SAR imaging plane is at or close to ground level then direct-target returns will have effective scattering centres above the imaging plane. These returns will appear focused at points displaced towards the radar (layover). Ground-target returns have effective scattering centres on the mean, ground reflecting surface, directly below the target centre. Ground-target-ground returns from raised targets have effective scattering centres below ground level, and consequently their returns display layover *away* from the radar in SAR images. Thus a SAR image of a target *in-situ* above a horizontal, dielectric surface appears combined of three separate images: a direct return displaying layover towards the radar, a ground-target return projected onto the reflecting, ground surface, and the ground-target-ground return with effective scattering centres displaying layover away from the radar. These three images are of differing overall brightness depending upon the reflecting properties of the ground surface. In general the ground-target-ground terms are the least bright as energy is lost in ground reflections.

E. Volume Scattering

The forest environment has been modelled using tree architecture models for Scots Pine, provided by Prof. Seppo Kelomäkki and Dr Veli-Pekka Ikonen at the Faculty of Forestry, University of Joensuu, Finland. These take the form of collections of dielectric cylinders, with detailed information concerning sapwood and heartwood dimensions, and needle distributions [16-18].

The forest is described using a map of tree positions and heights, and these heights are used to extract from the tree architecture database the tree model whose dimensions most closely match the tree at the location. The trees are placed in position above the ground surface described by the digital elevation model. Canopy inhomogeneity is accounted for by subdividing the canopy volume into smaller sub-volumes termed "voxels". Each voxel has dimensions commensurate with the SAR system resolution, and each contains many tree elements, which are subdivided on input to have dimensions well below the same resolution. Canopy effective permittivity is then mapped into voxels by examining voxel occupancy, and determining the contribution to mean permittivity from individual branch elements based upon knowledge of their dimensions, orientations and water contents. Note that that volume scattering events may be shadowed by targets in the same way as direct-ground scattering.

For direct forest clutter the effective scattering centre is taken to be the centre of the branch element, and the scattering amplitude is calculated using the truncated infinite cylinder approximation [15].

Note that there is no calculation of multipath *between* tree elements since this has in theory already been taken into account in the mean-field model: the local field at the scatterer is taken to be the mean field at that location, which estimate incorporates multiple scattering. This approximation is very much in keeping with the SAR imaging process: the mean field is coherent.

Needle scattering is estimated in a statistical manner, by simulating short random walks using a physical scattering model for needles, and scaling these short walks depending upon the number of needles associated with each branch element. Aside from the contribution of needles, calculation of direct tree scattering is purely deterministic.

Model ground-forest and ground-forest-ground calculations are limited to the case that the ground may be assumed locally flat (not curved), but roughened and tilted. The word "forest" in the following refers to any short element of the tree, be it in the trunk or stem, in the primary branches (those with origins in the stem), or in the secondary canopy. Ground-forest interactions have effective scattering centres located as the projection of the forest element centre in the locally flat, mean reflecting surface. The local, flat surface for each tree is determined by fitting to the digital elevation map in the vicinity of each tree. Similarly, ground-forest-ground interactions have effective scattering centres located below the reflecting ground surface at the reflection of the forest element centre in the locally flat, mean reflecting surface.

III. Description of Simulations

Predictions for forest clutter at L-band have been made for a forest stand with typical stem density. Predicted clutter levels at 45 degrees elevation of –4dB (HH) –11dB (HV) and –7dB (VV) are consistent with those reported in the open literature for similar forests [19].

At L-band, and to a lesser extent at UHF, the canopy under-storey vegetation may strongly affect direct-ground, ground-target/forest and ground-target/forest-ground returns. The proper incorporation of these effects, not modelled in the

work reported here, is underway. The option to model additional system noise, arising perhaps from RFI and incoherent returns, is available but has not been used in the current calculations. The validity of the GO-PO approximation at 23cm wavelength is open to question, however RCS estimates derived with this model are of the right order of magnitude, and the GO-PO approximation has been demonstrated to preserve the correct polarimetric scattering characteristics of known scattering primitives.

Simulations have been performed using two types of vehicle at different aspects. Both vehicles are large, being some 6m in length, 3m wide and almost 4m high at the tallest point. Fig. 1. indicates the vehicle arrangement in the forest as viewed from the simulated radar platform at the centre of the aperture.

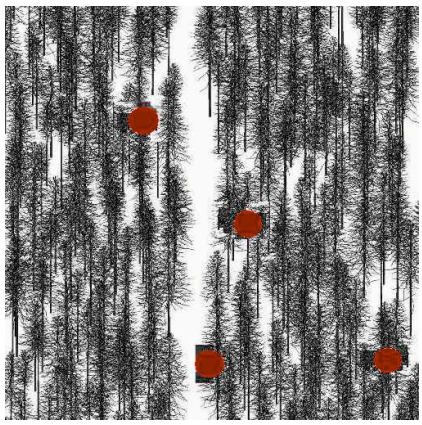

Fig. 1. Target vehicle deployment in the simulated scene as viewed from the radar platform. For the sake of clarity trees are depicted without secondary branches.

Calculations have been performed at L-band (wavelength 0.231m), simulating airborne radar at a ground range of 3km to image centre, and at 3km height above the minimum height of the DEM. The imaged area was 91m square, with pixels spaced at 0.5m. A Hamming weighted PSF was simulated with resolutions of 0.69m (width at half height power) in cross range and 1.38m in range, corresponding to a SAR bandwidth of 100MHz. Soil was modelled as moderately wet, with volumetric moisture content of 0.25 and dielectric permittivity of 12.6-*i*0.4. Soil surface roughness was 0.055m, and correlation length was 0.1510m. Wood permittivity ranged from 2.2-*i*0.4 (deadwood) to 26.8-*i*5.3 (sapwood) via 6.7-*i*1.9 (heartwood). Total attenuation by the canopy, comprised of trees of typical height 18m, was in the region of 4dB to 8dB depending upon polarisation.

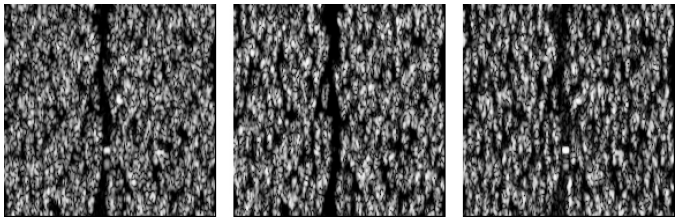

Fig. 2. Simulated HH (left), HV (centre) and VV (right) images of the forest scene with concealed targets, one of which is deployed on the central track. Each image is scaled to the mean for that channel (images are not equally bright).

The simulated SAR imagery is displayed in Fig. 2. Differences between channels are the result of tree architecture. Vertical trunks, containing a large proportion of the biomass, result in greater absorption of V over H polarised waves. At the same time primary and secondary branches are predominantly horizontal and scatter more H polarised energy back to the radar. The ground represents a rough dielectric, reflecting boundary, and at the incidence angle of 45 degrees, VV reflection coefficients are considerably less than HH. Thus ground-forest interactions appear much more strongly in HH than in VV, helping to increase the brightness of the HH image.

Target signatures are just visible in the HH image if one knows where to look, but not in HV and not always in VV. Without prior knowledge of target locations, target signatures, even in HH, are readily confused by clutter peaks. Attempting CFAR target detection on the HH channel will result in a large number of false alarms as we proceed to show.

IV. Analysis of Simulated Data

A. Single Channel CFAR

We have applied a straightforward CFAR detection to a single polarimetric channel. Since we have prior knowledge of target locations we can adjust the CFAR parameters in such a way as to minimise the false alarms, whilst maintaining detection of all four targets. CFAR parameters available for optimisation were the probability of false alarm (Pfa), the guard box size, and the size of the clutter box. In practice, because of high clutter levels, the best false alarm rate obtained using the HH channel, was of the order of 1/1000. This was obtained using a clutter box width of 21 pixels, and a guard box width of 11 pixels. The CFAR detection results are shown in the following figure.

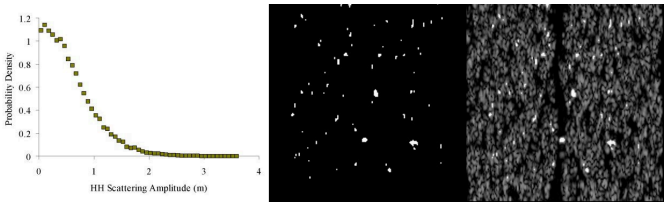

Fig. 3. Simulated HH clutter distribution (left), CFAR target detections (centre) and CFAR detections shown together with the full HH image. A false alarm rate of 1/1000 is the best that may be achieved with a single channel without loss of true target detections.

Whilst it is possible to detect the concealed targets, the large number of false alarms is highly undesirable from an operational point of view. Other information is clearly required in order to improve the false alarm rate. The

possibility of using detection clustering as another indicator is suggested by the CFAR results, however many of the false alarms belong to clusters of similar size to those connected with targets, and this information alone will not be sufficient.

B. Entropy-Alpha Decomposition

The four polarimetric channels were decomposed into entropy-alpha components, using the decomposition method of Cloude and Pottier [5]. The entropy component represents the relative contributions from each eigenvalue of the coherency matrix. Low entropy indicates that a single scattering mechanism is present, whilst high entropy indicates random scattering. The alpha component is derived from the phase of the eigenvectors and is indicative of the dominant scattering mechanism [5]. The decomposition was performed using 5 by 5 pixel box averaging, and the results of polarimetric decomposition are shown in Fig. 4.

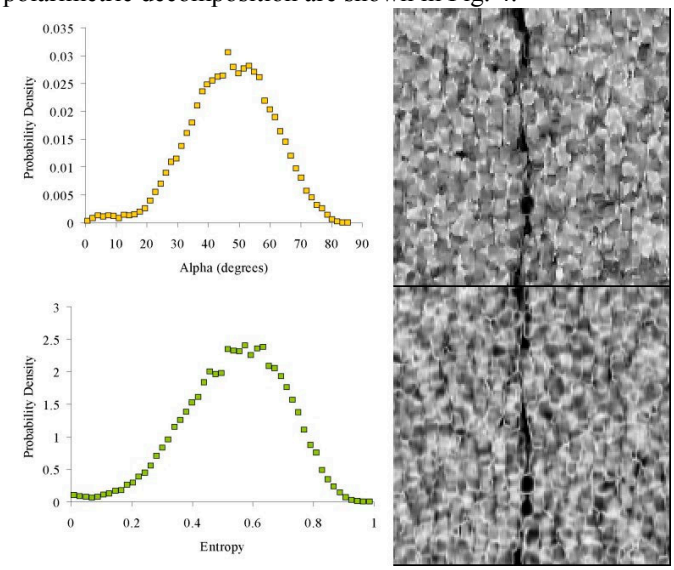

Fig. 4. Simulated HH alpha distribution (top-left) and alpha image (top-right), simulated HH entropy distribution (bottom-left)) and entropy image (bottom-right).

Both alpha and entropy distributions are approximately normal. Both have small but finite probability of low values associated with direct ground backscatter from the clear track in the centre of the forest stand. One vehicle was placed directly onto this track (see Fig. 1.) approximately one third of the way up the image in range. This vehicle is revealed in the images to have very low values of both alpha and entropy. This is consistent with scattering over the vehicle being characterised by a single, dominant scattering mechanism. Over the forested area the alpha and entropy values are distributed about means of approximately 45 degrees for alpha, corresponding to scattering from branches, and approximately 0.6 for entropy, indicating significant contribution from more than one scattering mechanism (ground-forest as well as direct-forest returns).

Thus low alpha and entropy values arise both from targets and ground surfaces, but rarely from forest clutter. Similarly, isotropic dihedral targets yield high alpha values, which are also rare in forest clutter. Ground returns are much smaller than target returns, so that low alpha and entropy coupled to high HH scattering amplitude is likely to arise from targets alone. We proceed to use this observation to discriminate between detected targets and false alarms.

C. Combined Single Channel CFARs

Standard CFARs were applied to both the alpha and entropy channels assuming normal clutter distributions. Each channel was inverted before application of the CFAR so that low entropy and alpha values were detected. Folding the alpha distribution about a midway point would permit detection of both high and low alpha values. The results of alpha and entropy channel CFARs were multiplied by the HH channel CFAR results in order to reduce false alarm rates. Rates for the alpha and entropy channels were reduced until a point was reached where any further reduction resulted in a loss of detection of one or more targets.

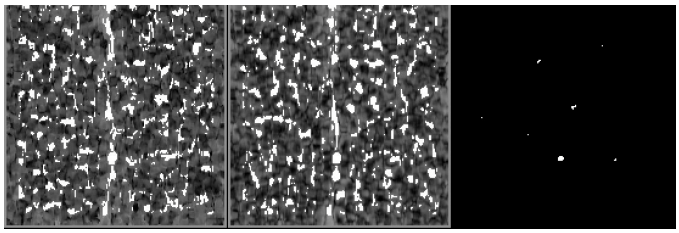

Fig. 5. Alpha CFAR hits displayed white on alpha clutter (left), entropy CFAR hits displayed white on entropy clutter (centre), and combined HH-alpha-entropy CFAR detection results. Only 3 isolated pixels show as hits not associated with targets with alpha and entropy Pfa set to 1/10.

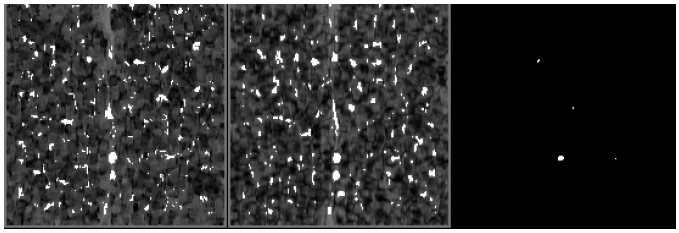

Fig. 6. Reduction of the alpha and entropy Pfa to 3/100 results in fewer alpha CFAR hits (left), and entropy CFAR hits (centre). The combined HH-alpha-entropy CFAR detection contains only target pixels, but one target is detected by only a single pixel.

With CFAR clutter and guard box sizes held constant a large Pfa threshold was required to preserve detection of all known targets. With the Probability of false alarm set to 1/10 in both alpha and entropy, large numbers of hits are recorded in both channels. However, when these CFAR results are combined simply with the HH channel the number of false alarms is reduced dramatically. In the original HH CFAR there are 313 recorded hits, of which at least 33 are associated with targets. Combining the HH and alpha CFARs results in a reduction in hits to 53. Combination of the HH CFAR with the

entropy CFAR yields 105 hits. Best of all, however, is the combination of the results of all three CFAR algorithms: this results in 36 hits, only 3 of which are not associated with targets (Fig. 5.). These three false alarms are isolated pixels and may be rejected by considering clustering effects. Further reduction of the alpha and entropy Pfa values to 3/100 results in no false alarms at all. However one target is detected using only one pixel (Fig. 6.).

V. CONCLUSION

We have developed a coherent, polarimetric SAR simulation and used simulated SAR imagery to demonstrate how polarimetric information might be used to improve target detection capability for concealed targets. The techniques described here for reduction of false alarms have used parameters optimised for this specific calculation. Whilst the result is limited to a single case of simulated data, we believe that a similar technique will have wider and more general applicability. The simulation is of a high fidelity, and the result indicates that further examination of the use of polarimetric data in target detection and identification is warranted.

ACKNOWLEDGMENT

The biologically accurate tree architectural models for Scots Pine used in this work have been provided by Prof. Seppo Kellomäki and Dr Veli-Pekka Ikonen of the Faculty of Forestry, University of Joensuu, Finland. The authors wish to express their sincere gratitude to Prof. Kellomäki and Dr Ikonen for their valuable gift of this data without which this, and much other work, would not have been possible.

REFERENCES

[1] M F Toups, L A Bessette and B T Binder, "Foliage Penetration Data Collections and Investigations Utilizing the P-3 UWB SAR", 1996, SPIE vol., 2757, p136.

[2] D Belcher, M L Williams, A Jones and K D Grover, DERA Internal Report, March 2000.

[3] Hellsten and L M H Ulander, Airborne Array Aperture UWB UHF Radar – Motivation and System Considerations, IEEE AES Systems Magazine, p.35, May 2000.

[4] L M H Ulander, P O Frolind and T Martin, Processing and Calibration of UWB SAR Data from CARABAS II, p273, Proc. CEOS SAR Workshop, Toulouse, 26-29 October, 2000

[5] S R Cloude and E Pottier, A Review of Target Decomposition Theorems in Radar Polarimetry, IEEE Trans. Geosci. Remote Sensing, vol.34, p498, Mar 1996.

[6] M L Williams, V Savage and C L Tham, Manuscript in preparation, November 2002.

[7] M L Williams and C L Tham, DERA Internal Report, March 2001

[8] M L Williams, A Study of Low Frequency SAR Clutter using Model Forests, Proceedings, International Geoscience and Remote Sensing Symposium, Honolulu, Hawaii, 24-28 July 2000.

[9] M L Williams, Simulation of Low Frequency SAR Clutter from a Pine Forest, EUSAR 2000, Munich, 24-28 May 2000.

[10] M L Williams, Prediction and Observation of SAR Clutter from Vegetation Canopies, Proceedings, International Geoscience and Remote Sensing Symposium, Hamburg, June 1999.

[11] M. L. Williams, Influence of canopy shape on SAR speckle distributions over woodland, Proceedings of the International Geoscience and Remote Sensing Symposium, Singapore, 3-8 August, IEEE, pp 755-757, 1997.

[12] M. L. Williams, S. Quegan and D. Blacknell, Distribution of backscattered intensity in the distorted Born approximation: application to C-band SAR Images of woodland, Waves in Random Media, 7, pp 643-660, 1997.

[13] M. L. Williams and S. Quegan, Modelling microwave backscatter from discrete random media using multiple-scattering series: convergence issues, Waves in Random Media, **7**, pp 213-227, 1996.

[14] M. L. Williams, Image statistics in the distorted Born approximation: application to C-band SAR images of dense woodland, Progress in Electromagnetics Research Symposium, p 627, Innsbruck, Austria, 8-12 July, 1996.

[15] A K Fung, Microwave Scattering and Emission Models and their Applications, Artech House, 1994.

[16] S. Kellomäki, Veli-Pekka Ikonen, Heli Peltola and Taneli Kolström, Modelling the Structural Growth of Scots Pine with Implications for Wood Quality, Ecological Modelling 122 (1999) 117-134.

[17] S. Kellomäki and Olavi Kurttio, A Model for the Structural Development of Scots Pine Crown based on Modular Growth, Forest Ecology and Management, 43 (1991) 103-123.

[18] S. Kellomäki and Harri Strandman, A Model for the Structural Growth of Young Scots Pine Crowns based on Light Interception by Shoots, Ecological Modelling 80 (1995) 237-250.

[19] A J Luckman and J R Baker, The Contribution of Trunk-Ground, Interactions to the SAR Backscatter from a Coniferous Forest, Proc. IGARSS, p2032, 1995.

[20] F T Ulaby and C Elachi (Eds.), Radar Polarimetry for Geoscience Applications, Artech House Remote Sensing Library, 1990.